JOURNAL OF MATERIALS SCIENCE 32 (1997) 1825–1833

Volume change during the solidification of SG iron: comparison between experimental results and simulation

QIMING CHEN
Materials Research Institute, Sheffield Hallam University, City Campus Pond Street, Sheffield S1 1WB, UK

E. W. LANGER, P. N. HANSEN*
*Metallurgy and *Thermal Processing of Materials, PI, Technical University of Denmark, 2800 Lyngby, Denmark*

In order to understand the shrinkage behaviour of spheroidal graphite (SG) iron during solidification, a volume change kinetic model was set up to simulate the volume change during the eutectic solidification, which was presented in an earlier paper. Furthermore in the present work experiments were carried out for comparison with theoretical prediction. The microstructure of the mushy zone during the solidification of SG cast iron was obtained by the quenching method and analysed by normal metallography and image analysis. The results show that the mushy zone exists in front of the interface between the liquid and the solid. The study by quantitative stereology shows that the graphite fraction in the mushy zone has the same trend as that of the theoretical prediction and the silicon content in cast iron strongly influences graphitization during the solidification. A heat-transfer model to stimulate the heat transfer of the experimental apparatus was developed. A modified Rappaz's model was used to simulate the eutectic growth under fully equilibrium conditions. The theoretical prediction has been compared with the experimental results, and found to be in good agreement with each other.

1. Introduction

Optimization of casting design to ensure the production of sound casting is particularly difficult in the case of ductile iron due to the complex solidification of the alloy and its extreme sensitivity to processing practice. This is because the specific volume of the solidified eutectic may be greater than that of the liquid from which it forms, because of the precipitation of graphite, which has a significantly lower density than iron. The specific volume of primary austenite changes significantly with temperature and composition [1, 2]. Furthermore, it is also quite difficult to predict the volume change, resultant mass flow and the kinetics that occur during freezing. Thus, fundamental considerations in numerical simulation-based shrinkage prediction research concerning spheroidal graphite (SG) iron are (i) the development of a kinetic model of SG iron solidification, which realistically accounts for the effects of metallurgical processing on the mode and sequence of solidification; and (ii) application of the model to estimating the volume changes occurring during freezing [3]. Furthermore, the volume change kinetics can be coupled to the fluid flow model and the eutectic expansion effect model so that the casting defect of SG iron can be predicted with a clearly physical model as a whole. However, the first thing we can do is to set up a volume change kinetic model to describe the process of the volume change during the eutectic solidification. There are two approaches that have been taken in simulating the solidification behaviour of SG iron, e.g. microstructural modelling [4, 5] based on fundamental nucleation and growth consideration and thermal analysis. However, we concentrate on the former approach e.g. microstructural modelling based on fundamental nucleation and growth of SG cast iron.

In earlier research, a eutectic solidification model of SG iron with volume change has been proposed [6] and the influence of nucleation and growth on the volume change during the eutectic reaction has been studied with this model [7]. In this paper, experimental work to observe the interface structures between the solid and liquid and the mushy zone feature is presented. On the other hand, a one-dimensional heat-transfer model is employed to describe approximately the heat transfer of the experimental facility. The modified Rappaz growth model described elsewhere [8] and volume change model [6] are coupled to this heat-transfer model. A computer program has been developed to simulate the structure development near the interface between liquid and solid during the eutectic solidification. Because the change of graphite

0022–2461

fraction during eutectic solidification is the main reason for the volume change, the results of the simulation of the graphite fraction are compared with the experimental results of the graphite fraction, and they are found to match reasonably well.

2. Mathematical model

2.1. Heat-transfer model

Under the conditions which are described in Section 3, a high-frequency heating facility was employed to maintain the liquid part of sample at a given temperature. After pouring the liquid iron into the mould, the solidification starts from the bottom of the mould and progresses to the interface between the heated part and unheated part of the sample, as shown in Fig. 1. Furthermore, we assume that the effect of heating by electro-magnetic induction in the solid part below the interface between the solid and liquid, can be neglected.

Based upon this physical situation the following control equation and boundary condition is proposed [9] to simulate the process. For simplicity, a one-dimensional finite difference method (FDM) is employed, which is valid assuming the heat flow is one dimensional and the convective and radiative heat flow are neglected. The time-dependent form of the heat transfer can be described as follows

$$k\frac{\partial^2 T}{\partial x^2} + L\frac{\partial f_s}{\partial t} = \rho C_p \frac{\partial T}{\partial t} \tag{1}$$

where T is temperature, x is distance, k is thermal conductivity, ρ is material density, C_p is specific heat, f_s is solid fraction and t is time.

The boundary condition is as follows

$$\text{at} \quad x = l,\ \dot{q} = 0; \quad \text{at } x = 0,$$

$$h_{\text{interface}}(T_S^{\text{metal}} - T_S^{\text{mould}}) = k\left(\frac{\Delta T}{\Delta x}\right) \tag{2}$$

at the mould outer surface,

$$h(T_S^{\text{mould}} - T_{\text{amb}}) = k\left(\frac{\Delta T}{\Delta x}\right) \tag{3}$$

and the initial conditions are

$$\text{at} \quad t = 0, \quad T = T_{\text{soak}}, \tag{4}$$

where l is the length of the sample below the liquid zone as shown in Fig. 1, $\dot{q}$ is heat flux rate and $h_{\text{interface}}$ is the heat-transfer coefficient between the sample and the steel mould, and h is the heat-transfer coefficient between the steel and ambient

$$h = \varepsilon\Gamma F(T_S^{\text{mould}\,2} + T_{\text{amb}}^2)(T_S^{\text{mould}} + T_{\text{amb}}) \tag{5}$$

where ε is the radiation factor, F the shape factor and Γ is the Stefan–Boltzmann constant (5.669×10^{-8} $\text{W m}^{-2}\text{K}^{-4}$). T_S^{mould} is the temperature of the steel mould and T_{amb} is ambient temperature. A fully implicit scheme was used. The details about discreting and coupling between the sample and the steel mould are described in Appendix 1.

2.2. Kinetic model of eutectic solidification

The detail of the kinetic model of the eutectic solidification has been described elsewhere [6]. Here we only give a brief description as follows:

(i) Oldfield's nucleation model;

(ii) Rappaz's and Su's diffusion model of growth of spheroidal austenite and graphite. The nucleation model is based on experimental results and the growth model is based on Fick's law of quasi-steady diffusion and considers the solute and mass balance in the eutectic domain. Both of them are functions of the undercooling. A detailed discussion of the models was presented elsewhere [7].

2.2.1. Nucleation model

$$N = A_n \Delta T^n \tag{6}$$

where A is the nucleation constant, N the nucleation number per unit volume, ΔT the undercooling, $n = 1$ or 2, depending on the effectiveness of inoculation, and

$$\frac{dN}{dt} = A_n n \Delta T^{n-1}\frac{d(\Delta T)}{dt} \tag{7}$$

2.2.2. Growth model for the eutectic cell

A modified Rappaz's model [8] was used as follows

$$\frac{dR_G}{dt} = \frac{\dfrac{D_C}{R_G}\dfrac{C_A - C_G}{1-(R_G/R_A)}}{\left[\dfrac{\rho_G}{\rho_A}(100 - C_{L,\text{aver}}) + (C_{L,\text{aver}} - C_G)\right]} \tag{8}$$

$$\frac{dR_A}{dt} = \left[\frac{D_C}{R_A}\frac{C_G - C_A}{1-(R_A/R_G)} + \frac{\rho_L}{\rho_A}\frac{dC_L}{dt}F(\beta, R_A, R_G)R_A\right]\Big/(C_{L,\text{aver}} - C_A), \quad (R_0 - R_A > \beta(R_A - R_G), \beta \geq 0) \tag{9}$$

$$\frac{dR_A}{dt} = \left[\frac{D_C}{R_A}\frac{C_G - C_A}{1-(R_A/R_G)} + \frac{\rho_L}{\rho_A}\frac{dC_L}{dt}F(\beta, R_0, R_A, R_G)R_A\right]\Big/(C_{L,\text{aver}} - C_A), \ (R_0 - R_A < \beta(R_A - R_G), \beta > 0) \tag{10}$$

where R_0 is the equivalent radius of the eutectic domains R_A, R_G are the radii of austenite shell and graphite nodule, respectively. C_A, C_G are the carbon contents (wt %) at the interface between austenite and liquid, and austenite and graphite, respectively;

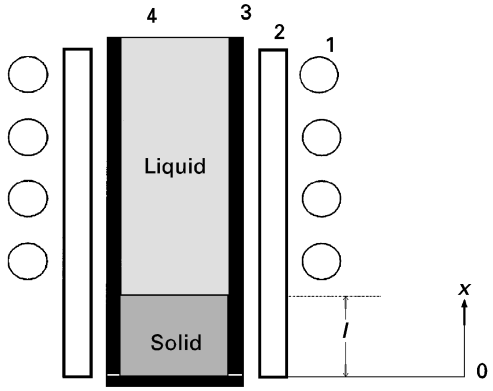

Figure 1 Modelling of heat transfer of the sample and its boundary conditions in the heating facility. 1, High-frequency coil; 2, insulating materials; 3, stainless steel mould; 4, sample.

$C_{L,aver}$ is the average carbon content of residual liquid during eutectic reaction and

$$\frac{dC_L}{dt} = \frac{1}{m_{BC}}\frac{dT}{dt} \quad (11)$$

where m_{BC} is the slope of the austenite liquidus. In numerical calculation, $C_{L,aver}$ is obtained from

$$C_{L,aver} = C^B_{L,aver} + \Delta C_{L,aver} \quad (12)$$

where B indicates the previous time step. A boundary layer factor β ($\beta > 0$) may be used to modify the thickness of the solute boundary layer, and $F(\beta, R_A, R_G)$ and $F(\beta, R_0, R_A, R_G)$ are the functions which were described elsewhere [8] in detail.

The formulas developed by Su *et al.* [10] as follows have also been used for comparison

$$\frac{dR_A}{dt} = D_C\frac{(C_G - C_A)}{(C_L - C_A)}\left[R_a\left(\frac{R_A}{R_G} - 1\right)\right]^{-1} \quad (13)$$

$$\frac{dR_G}{dt} = D_C\frac{\rho_A}{\rho_G}\frac{C_A - C_G}{100 - C_G}\left[R_G\left(1 - \frac{R_A}{R_G}\right)\right]^{-1} \quad (14)$$

and a detailed discussion of the difference between the two models was given previously [7]. Thus, the corresponding fractions of graphite and austenite can be calculated.

2.2.3. Correction of the solid fraction after the eutectic reaction

After the eutectic reaction, f_G and f_A will be modified using the formula below, because the carbon content in austenite is precipitated

$$dR_G = \frac{\rho_A}{\rho_G + \rho_A C_{aver}} dC_{aver}\frac{(R_A^3 + R_G^3)}{3R_G^2} \quad (15)$$

where C_{aver} is the average carbon content and can be obtained as follows

$$C_{aver} = C_{A,max} - \left[\frac{3}{2}\left(\frac{R_A}{R_G} + 1\right)\Big/\left(\frac{R_A^2}{R_G^2} + \frac{R_A}{R_G} + 1\right)\right] \times (C_A - C_G) \quad (16)$$

The corresponding R_G is

$$R_G = R^B_G + \Delta R_G \quad (17)$$

where B indicates the value of the last time step. The corresponding Δf_G can be calculated from

$$\Delta f_G = \frac{4}{3}\pi N (R_G^3 - R_G^{B3}) \quad (18)$$

and f_G and f_A can be modified by

$$f_A = f^B_A - \Delta f_G \quad (19)$$

$$f_G = f^B_G + \Delta f_G \quad (20)$$

and f_G will increase and f_A will decrease after the eutectic reaction, which will be used to calculate the volume change during the solidification of SG cast iron.

2.3. Volume change model

It is assumed that at a given time the density of the mushy zone is an average density of a mixture which consists of liquid, graphite and austenite without others phases forming

$$\rho_{mixture} = f_L\rho_L + f_G\rho_G + f_A\rho_A \quad (21)$$

where f, ρ stand for volume fraction and density, L, G and A represent liquid, graphite and austenite, respectively.

The calculation methods of densities of austenite, graphite and liquid and volume change as well as coupling the volume change model to the growth kinetic model, have been described in detail elsewhere [6].

3. Experimental investigation of the structures of the mushy zone during solidification of cast iron

Cast iron is an Fe–C–Si ternary alloy. During the solidification of cast iron, the eutectic reaction occurs in a temperature range where solid and liquid exist at the same time. The volume with a mixture of solid and liquid in front of the solidification front is called the mushy zone. Several previous investigations confirmed the existence of the mushy zone during the solidification of grey iron with the pour-out and quench methods [11, 12], but they did not give any information about the volume change in the mushy zone and the influence of temperature and inoculation on the volume change of the mushy zone during the eutectic reaction.

For SG cast iron the eutectic reaction and the corresponding volume change occurs in the mushy zone. Therefore, it is important to investigate the evolution of the microstructure during the eutectic solidification of SG cast iron in the mushy zone. In this investigation, a specially designed heating facility was employed to obtain the structures near the interface between the solid and liquid.

TABLE I The compositions of the pig irons (wt %)

Sample	C	Si	Mn	P	S
F7–F9	3.62	2.16			
F10–F16	3.92	1.05	0.012	0.0022	0.006

TABLE III Composition of the colour etching reagent (wt %)

KOH	NaOH	Picric acid	Distilled water
18	9	9	Balance

3.1. Experimental procedure

3.1.1. Raw materials

The raw materials chosen were pig iron with the composition given in Table I. NiMg alloy was employed as spheroidization agent with 15 wt %Mg and FeSi alloy with 75% Si as inoculant.

3.1.2. Equipment

A simple heating apparatus was developed as shown in Fig. 1. It is composed of an induction coil of copper tube cooled by water. A high-frequency power unit was used to heat the casting.

3.1.3. Chemical composition of the samples

The chemical compositions of the samples are shown in Table II with the trace elements of tin, molybdenum and aluminium. The carbon content was analysed by a special CS instrument and other elements were analysed by spectrometry.

3.1.4. Preparation of the samples

Pig iron was melted in a high-frequency furnace. After the temperature of furnace was raised to 1300 °C, the melt was spheroidized and inoculated in the furnace with 0.8%–1.0% NiMg alloy and 0.5%–1.5% FeSi alloy, respectively. Then the melt was poured into a 33 mm steel tube mould heated to 1000 °C before pouring, and the steel mould was put into the heating apparatus for immediate heating. After the lower part of the sample, which was outside the coil of heating equipment, was solidified, the stainless steel tube mould was quenched in water. The sample was sectioned longitudinally, ground on water-lubricated silicon carbide paper down 1000 grade, and finally polished using diamond (7–1 μm) for metallographic examination and image analysis. The sample was sectioned transversely and ground for chemical analysis.

A colour etching method [13–15] was also employed using picric acid solution to distinguish the eutectic austenite from the primary austenite. The ingredients of the solution are shown in Table III.

4. Results and discussion

4.1. Structure of the interface between the solid and the liquid

The macrostructure of the interface between the solid and the liquid is shown in Fig. 2 for nodular iron. When the heating power is small, the interface surface tends to be a plane. The samples were etched in 5% nital.

The quenching microstructure of the interface between the solid and the liquid for nodular iron is shown in Figs 3 and 4. At the solid side, the quenched structure is composed of martensite, austenite, bainite and graphite. It was reported that for the normal solidification of SG iron, the pro-eutectic austenite can be distinguished from the eutectic austenite by a colour-etching method [13]. Because the method cannot reveal a distinction between the proeutectic austenite and the eutectic austenite for the quenched structure, we cannot obtain information about the

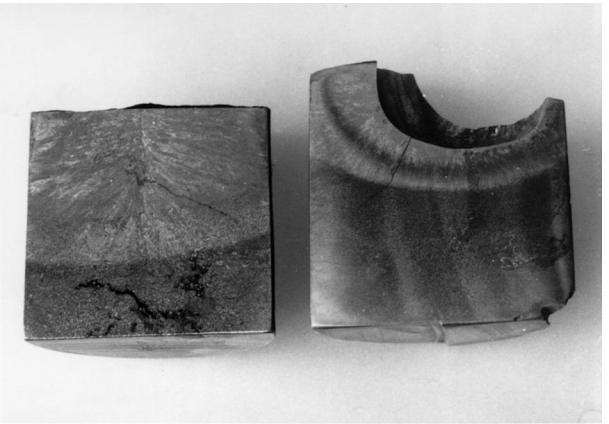

Figure 2 Macrostructure of the interface between the liquid and the solid of nodular iron.

TABLE II Compositions of the samples (wt %)

Sample	C	Si	Mn	P	S	Mg	Ni	Cu	Cr	CE
F5	3.11	1.80	0.404	0.054	0.0204	–	0.053	0.093	0.046	3.704
F7	3.74	2.08	0.030	0.017	0.0210	0.066	1.094	0.041	0.008	4.426
F8	3.66	2.43	0.008	0.012	0.0033	0.065	1.017	0.020	0.000	4.463
F9	3.80	2.07	0.030	0.020	0.0210	0.068	1.023	0.038	0.013	4.421
F10	3.50	0.77	0.030	0.038	0.0230	0.041	0.892	0.041	0.028	3.731
F11	3.90	1.36	0.030	0.029	0.0210	0.037	0.693	0.027	0.028	4.319
F12	3.87	1.45	0.040	0.032	0.019	0.045	0.838	0.025	0.041	4.305
F13	3.84	1.55	0.030	0.024	0.024	0.053	0.074	0.025	0.024	4.305
F15	3.75	1.95	0.030	0.028	0.019	0.053	0.893	0.027	0.027	4.335
F16	3.76	1.96	0.030	0.028	0.019	0.049	0.917	0.026	0.026	4.348

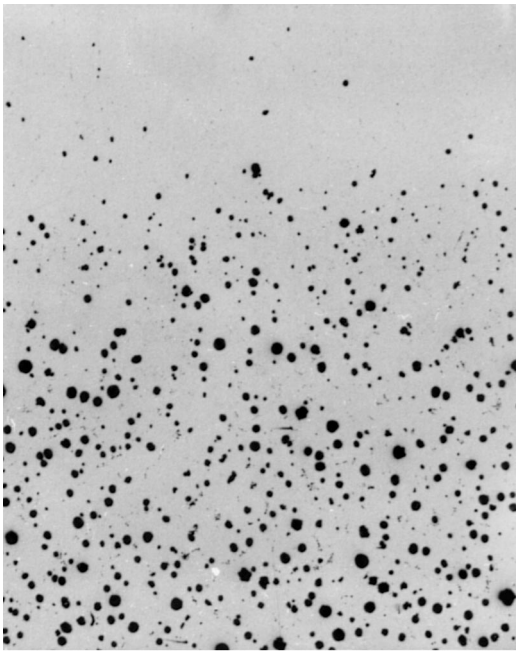

Figure 3 Interface structure, sample F11, polished, ×33.

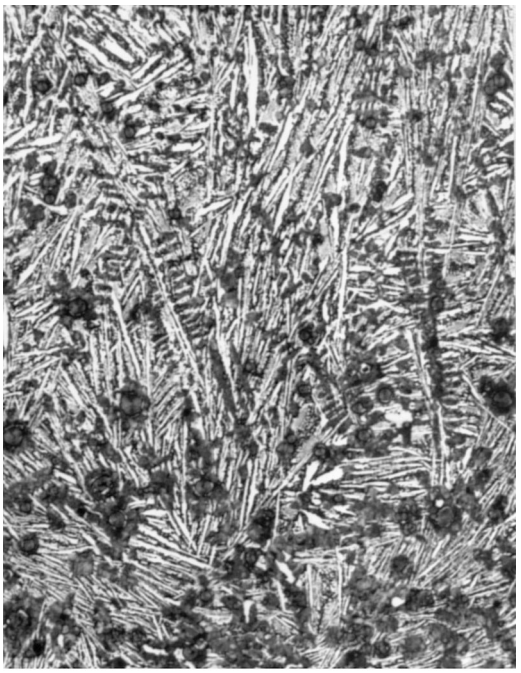

Figure 4 Sample F11, etched in 1% nital, ×64.

ratio between the radii of austenite and graphite. However, the connection of the pro-eutectic austenite growth and the eutectic growth can be seen. The arrangement of graphite has the same orientation as that of the austenite dendrites. The development of the eutectic cell strongly depends on the development of pro-eutectic austenite; meanwhile the development of austenite depends on chemical composition and cooling conditions. Therefore, even for a ductile iron with eutectic carbon equivalent, for example F11, well-developed pro-eutectic austenite will appear. This is because a lower silicon content suppresses the stable eutectic transformation and promotes the meta-stable eutectic transformation. The mushy zone can be seen near the interface between the solid and the liquid, in which the sizes of graphite nodules change gradually. The width of the mushy zone is narrow because of the large temperature gradient in the mushy zone. Most graphite nodules in the mushy zone are covered by austenite shell and mixed with the liquid quenching structure (fine austenite dendrites and cementite as well as ledeburite).

4.2. Image analysis of the mushy zone structures

The prepared polished samples were measured using Global Lab Image and Global Lab Acquire Software and the corresponding optical system. Measurement was carried out on the areas through the liquid to the solid interface by taking fields in turn. Each point is the average value of five measurements at different locations, obtained by moving the fields parallel to the interface.

The original data from the measurement are the mean area of graphite, A_M, and the number of graphite nodules, N_A, on the screen. Therefore, the volume fraction of graphite can be obtained by [16]

$$f_G = f_A \tag{21}$$

where f_A is the area fraction of graphite

$$f_A = A_M \cdot N_A \tag{22}$$

From the Saltykov equation [17]

$$N_V = 2.38\, N_A^{1.6} \tag{23}$$

the number of nodules per unit volume, N_V, can be obtained, where N_A is the number of nodules on the section surface of the sample. The magnification effect [17], which refers to the fact that measurements made on the same microstructure at different magnifications yield different results, is not significant for our measurement (see Table IV) because the magnification used was rather lower than that used elsewhere [12].

A typical result of sample 7 is shown in Fig. 5. It is obvious that the fraction of graphite of the samples shows the same trend. The fraction of graphite on the solid side with the eutectic carbon equivalent (CE) is in good agreement with that from equilibrium conditions ($f_G = 0.067$–0.068) for the eutectic CE. The numbers of graphite nodules of the samples are different because of the different effectiveness of inoculation and chemical composition. The graphitization degree

TABLE IV Influence of magnification on the measurement parameters

Objective (×)	Mean area (μm²)	Average radius (μm)	No. of graphite	f_G
plane4 (300×)	330.2	10.02	147	0.069 96
epi8 (600×)	336.5	9.97	148	0.070 76

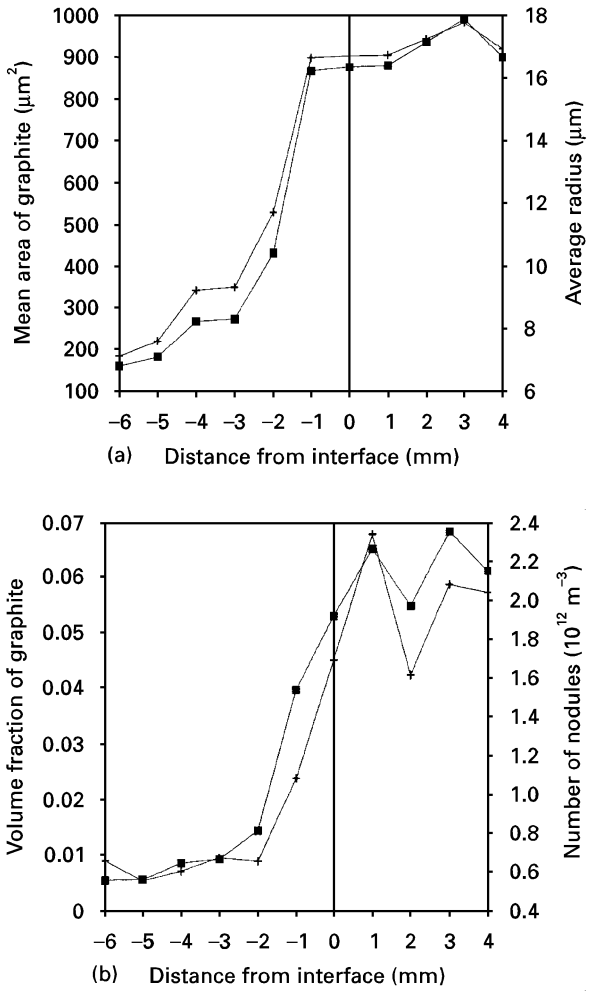

Figure 5 (a) (■) Mean area and (+) average radius, and (b) (■) volume fraction of graphite and (+) number of nodules per unit volume, for sample F7.

is a result of the nucleation and growth conditions of the graphite nodules. The influence of the silicon content and the carbon equivalent on the graphitization degree are evident, as is shown in Figs 6 and 7.

4.3. Comparison between the experimental results and the prediction of the theoretical model

The calculation was carried out under the following conditions: $l = 0.025$ m, $T_{amb} = 25\,^{\circ}C$, $T_{soak} = 1200\,^{\circ}C$. The solid correction was employed before the eutectoid temperature (for sample F8 it is 840 °C, which was also the quenching temperature in the experiment). A proper nucleation constant was chosen so that the eutectic cell number was identical to that of the experimental result as shown in Fig. 8.

It is difficult to obtain information on volume change in the mushy zone directly from the experiment. However, because the volume change is decided by the amount of graphite during the solidification, the data of the graphite fraction near the interface in the mushy zone, which are closely related to the volume change of the eutectic domain, were collected and plotted versus distance from the interface. The development of the interface during the eutectic solidification is shown in Figs 9 and 10 with the modified Rappaz's and Su's models, respectively, for the condition of sample F8. After 300 s, the liquid–solid interface tends to a stable position near the heating front of the heating apparatus. With the different growth models of Su and Rappaz, the trends of the graphite fraction towards the solid side of the interface are the same. The solidification tends to the equilibrium state and the element near the interface obtains a higher graphite fraction while the element far from interface (solid side) obtains a slightly lower graphite fraction. This is because the graphite precipitated during the cooling after the eutectic reaction is considered here by the model of solid fraction correction described elsewhere [5].

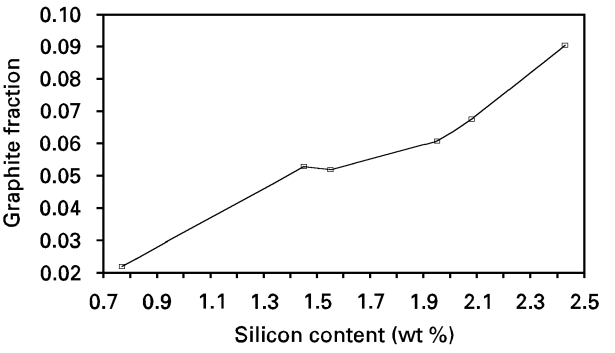

Figure 6 Relationship between silicon content and graphitization of SG iron.

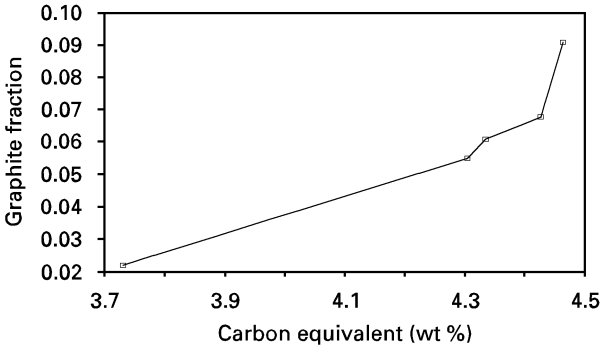

Figure 7 Relationship between carbon equivalent and graphitization.

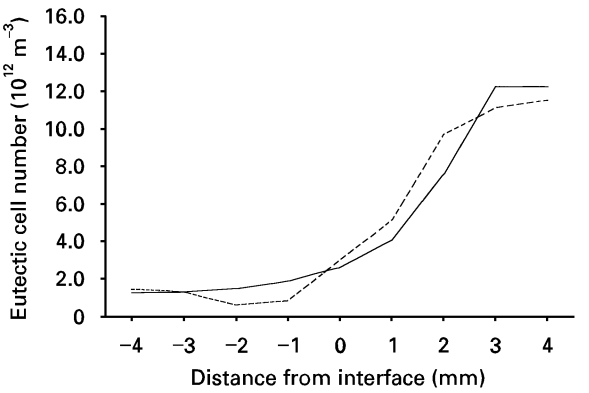

Figure 8 Comparison of eutectic cell number near the mushy zone during the eutectic solidification of SG iron between (——) simulation and (– – – –) experimental results (sample F8, 3.66%C, 2.43%Si, 200 s).

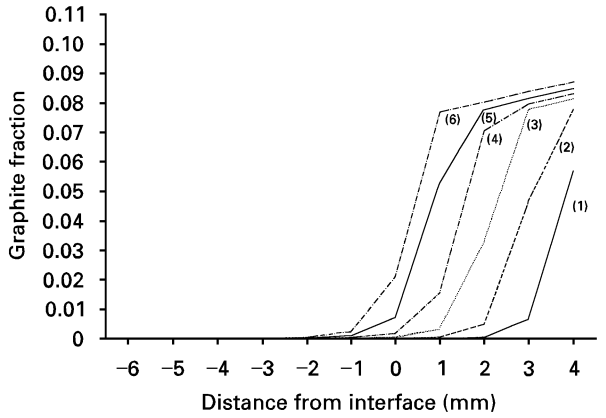

Figure 9 Graphite fraction near the mushy zone during the eutectic solidification of SG iron by the modified Rappaz's model, simulating the condition of sample F8. Time: (1) 50 s, (2) 100 s, (3) 150 s, (4) 200 s, (5) 250 s, (6) 286 s.

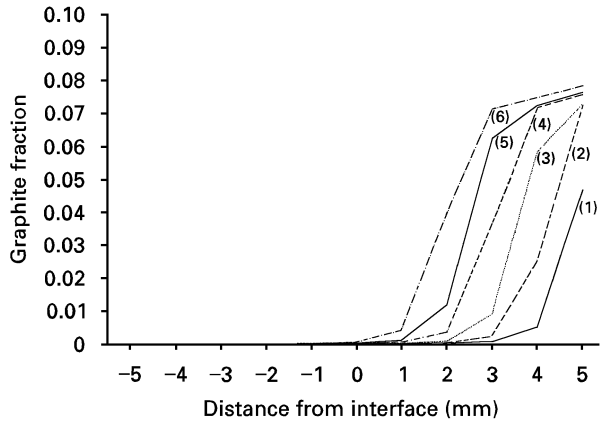

Figure 10 Graphite fraction near the mushy zone during the eutectic solidification of SG iron by Su's model, simulating the condition of sample F8. Time: (1) 50 s, (2) 100 s, (3) 150 s, (4) 200 s, (5) 250 s, (6) 300 s.

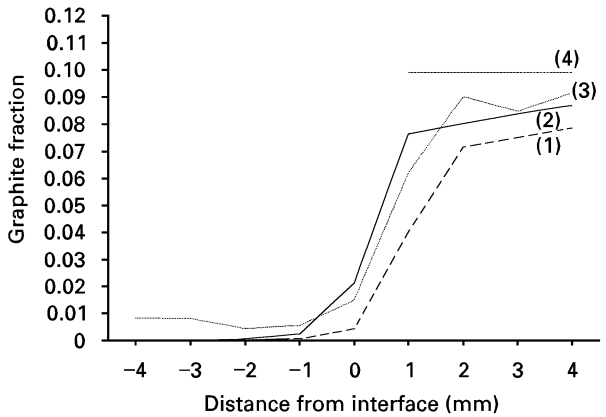

Figure 11 Comparison between the experimental result (sample F8) and theoretical prediction; 300 s. (1) Su's model, (2) Rappaz's model, (3) experiment, (4) equilibrium.

A comparison of the experimental and simulation results is shown in Fig. 11. Obviously the theoretical prediction by the modified Rappaz's and Su's models exhibit the same trends as that of the experimental results. Assuming that only the precipitation of graphite *before* the eutectoid is considered, the graphite fraction should be a constant which is the sum of the graphite precipitated during the eutectic reaction and the graphite precipitated during the cooling after the eutectic reaction.

The graphite fraction precipitated during these two stages can also be evaluated by the Fe–C–Si equilibrium diagram, as shown in Appendix 2. The results are compared with the prediction of Rappaz's model and the experimental results in Fig. 11. Therefore, the prediction of Rappaz's model fits the experimental result reasonably well. In practice the solidification of SG iron in a sand mould is in an equilibrium condition owing to the high heat resistance of the mould. So Rappaz's growth model is very suitable for employing to simulate the solidification process if the volume change must be considered, especially for predicting porosity formation.

5. Conclusion

The results show that there is a physical volume in front of the interface between the liquid and the solid in which a mixed structure of liquid and solid exists. The study by quantitative stereology shows that the graphite fraction in the mushy zone has the same trend as is theoretically predicted. The influence of silicon composition on the graphitization is significant. Under the fully equilibrium condition, the modified Rappaz's model is in very good agreement with the experimental results. Further work on the calculation of the expansion force can be carried out because a model for the expansion force accompanying the freezing of SG iron has been proposed [18].

References

1. R. W. HEINE, *AFS Trans.* **96** (1988) 413.
2. QIMING CHEN, E. W. LANGER and P. N. HANSEN, *Scand. J. Metall.* **23** (1994) 3.
3. F. J. BRADLEY, in "Modelling of casting, welding and Advanced Solidification Processes V", edited by M. Rappaz, M. R. Ozgu and K. W. Mahin (The Minerals, Metals and Materials Society, Warrendale, Pennsylvania, 1991) p. 177.
4. M. RAPPAZ and D. M. STEFANESCU, "Metals Handbook", 9th Edn, Vol. 15, edited by D. M. Stefanescu, "Casting" (ASM, Metals Park, Ohio, 1988) p. 883.
5. M. RAPPAZ, *Int. Mater. Rev.* **34** (1989) 94.
6. QIMING CHEN, E. W. LANGER, P. N. HANSEN, *Scand. J. Metall.* **24** (1995) 48.
7. *Idem.*, *ibid.* **24** (1995) 3.
8. *Idem*, in "Proceedings of the Modelling Casting, Welding and Advanced Solidification Processes VII", edited by M. Cross and J. Campbell (TMS, Warrendale, Pennsylvania, 1995) p. 633.
9. D. K. BANERJEE and D. M. STEFANESCU, *AFS Trans.* **99** (1991) 747.
10. KOU-CHANG SU, I. OHNAKA, I. YAMAUCHI and I. FUKUSAKO, *Mater. Res. Symp.* **34** (1985) 181.
11. W. OLDFIELD, *BCIRA J. Res. Devel.* **8** (1960) 177.
12. S. ENGLER and M. DETTE, in "The Metallurgy of Cast Iron", edited by B. Lux, I. Minkoff and F. Mollard (Georgi, St. Saphorin, Switzerland, 1975) p. 697.
13. S. M. A. BOUTORABI and J. CAMPBELL, *Mater. Charact.* **31** (1993) 127.
14. WANG YIQING, FAN ZHIKANG, GAN YU and ZHU XIANHUA, in "Conference Proceedings, Cast Iron IV" edited by G. Ohira, J. Kusakawa and E. Niyama (MRS, Pittsburgh, PA, 1990) p. 95.
15. HUAMENG TIAN and M. STEFANESCU, *Mater. Charact.* **29** (1992) 329.
16. E. E. UNDERWOOD, "Stereology and Quantitative Metallography", ASTM STP 504 (American Society for Testing and Materials, Philadelphia, PA, 1972) p. 3.

17. *Idem*, "Practical Applications of Quantitative Metallography", ASTM Special Technical Publication 839 (American Society for Testing and Materials, Philadelphia, PA, 1984) p. 160.
18. E. FRAS and H. F. LOPEZ, *AFS Trans.* **102** (1994) 597.
19. P. J. WRAY, *Metall. Trans.* **7B** (1976) 639.
20. J.-M. THERET and G. LESOULT, *Hommes et Fonderie* February (1984) 19.

Appendix 1. Finite difference equation

1. Finite difference equation for the inner nodal

If

$$F_0 = \frac{k\,\Delta t}{\rho C_p \Delta x^2} \tag{A1}$$

one has the finite difference equation for the inner nodal

$$-T_{i-1} + \left(2 + \frac{1}{F_0}\right) T_i - T_{i+1} = \frac{1}{F_0'} T_i' \tag{A2}$$

The increment of temperature resulting from the increment of fraction of solid during the solidification can be expressed as

$$T_i' = T_i^{B'} + \Delta T_{\text{incre}} \tag{A3}$$

where $T_i^{B'}$ is the temperature corresponding to the previous time step and

$$\Delta T_{\text{incre}} = \frac{L \Delta f_s}{C_p} \tag{A4}$$

Let

$$WM_i = \frac{1}{F_0} \tag{A5}$$

where F_0 is the Fourier number as a function of temperature, and L is the latent heat which is released from unit mass ($J\,kg^{-1}$). Thus we have

$$-T_{i-1} + (2 + WM_i) T_i - T_{i+1} = WM_i T_i' \tag{A6}$$

2. Finite difference equation for the centre nodal

The finite difference equation is

$$2k\left(\frac{T_{2'} - 2T_1 + T_2}{\Delta x^2}\right) = \rho C_p \frac{T_1 - T_1'}{\Delta t} \tag{A7}$$

Because of symmetry, $T_{2'} = T_2$ and one has

$$(4 + WM_1) T_1 - 4T_2 = WM_1 T_1' \tag{A8}$$

where $T_1 = T_{\text{soak}}$.

3. Finite difference equation for the boundary

Coupling the boundary nodals between the iron and steel mould

If the boundary nodal of the iron side is M and that of the mould side is nodal $M + 1$, and considering the energy balance at the boundary nodal M, $M + 1$, respectively, we have the following finite difference equations for the boundary nodals M, $M + 1$.

If

$$F_{0,\,\text{mould}} = \frac{k_{\text{mould}}\,\Delta t}{\rho_{\text{mould}} C_{p,\,\text{mould}} \Delta x_{\text{mould}}^2} \tag{A9}$$

$$WM_{i,\,m} = \frac{1}{F_{0,\,\text{mould}}} \tag{A10}$$

we have for the iron side, M

$$-T_{M-1} + \left(1 + WM_M + \frac{h_{\text{interface}}\,\Delta x}{k}\right) T_M - \frac{h_{\text{interface}}\,\Delta x}{k} T_{M+1} = WM_M T_M' \tag{A11}$$

for the mould side, $M + 1$

$$-\frac{h_{\text{interface}}\,\Delta x_{\text{mould}}}{k_{\text{mould}}} T_M + \left(1 + WM_{M+1,\,m} + \frac{h_{\text{interface}}\,\Delta x_{\text{mould}}}{k_{\text{mould}}}\right) \times T_{M+1} - T_{M+2} = WM_{M+1,\,m} T_{M+1}'. \tag{A12}$$

Inner nodal of the steel mould

$$-T_{i-1} + (2 + WM_{i,\,m}) T_i - T_{i+1} = WM_{i,\,m} T_i'. \tag{A13}$$

where $M + 1 < i < N$ and M is the boundary nodal of iron and N is the surface nodal of the steel mould.

The boundary between mould and ambient

If T_{amb} and T_N are the temperatures of ambient and the interface between the mould and air we have the boundary condition as follows.

If

$$Bi = \frac{h\,\Delta x_{\text{mould}}}{k_{\text{mould}}} \tag{A14}$$

we have

$$-T_{N-1} + (1 + WM_{N,\,m} + Bi) T_N = WM_{N,\,m} T_N' + Bi T_{\text{amb}} \tag{A15}$$

Appendix 2. Evaluation of the graphite fraction from the equilibrium diagram

The evaluation of the graphite fraction can be made from the equilibrium diagram of the Fe–C–Si alloy. Using sample F8 (3.64%C, 2.43%Si) for instance, the part of Fe–C–Si diagram is shown in Fig. A1 calculated by Thermo-Calc. The values of the carbon saturation point in austenite at the eutectic and the eutectoid temperatures are 1.85% and 0.56%, respectively. Furthermore, we have

$$g_A = \frac{100 - 3.64}{100 - 1.85} = 0.981\,76 \tag{A16}$$

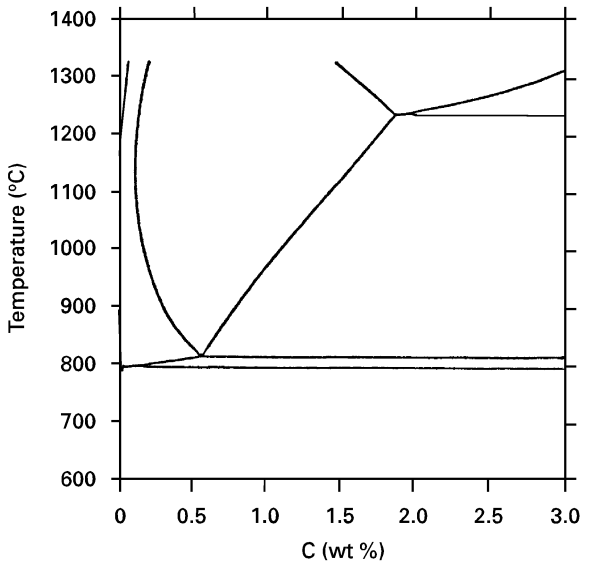

Figure A1 Part of the equilibrium diagram of Fe–C–Si alloy calculated by Thermo-Calc.

where g_A is the mass fraction of austenite for the eutectic reaction, and

$$g'_A = \frac{100 - 1.85}{100 - 0.56} = 0.987\,03 \qquad \text{(A17)}$$

where g'_A is mass fraction of austenite just before the eutectoid reaction.

The mass fraction can be converted to volume fraction by [19]

$$f_A = \left[1 + \frac{\rho_A}{\rho_G}\left(\frac{1}{g_A} - 1\right)\right]^{-1} \qquad \text{(A18)}$$

where f_A is the volume fraction of austenite, ρ_A and ρ_G are the densities of austenite and graphite, respectively. For the eutectic, ρ_A is $7000\,kg\,m^{-3}$, ρ_G is $2080\,kg\,m^{-3}$ [1]. For the eutectoid, ρ_A is $7200\,kg\,m^{-3}$, ρ_G is $2270\,kg\,m^{-3}$ [20]. As a result, we have

$$f_{G,\,total} = f_G + f'_G = 0.058\,846 + 0.040\,353 = 0.099\,199 \qquad \text{(A19)}$$

where $f_{G,\,total}$ is the volume of the total graphite that includes the volume fractions of graphite, both eutectic , f_G, and before the eutectoid, f'_G.

Received 19 January
and accepted 17 September 1996